CERN-INTC-2006-006
INTC-P-204

Proposed study of the neutron-neutron interaction at the CERN nTOF facility

P.A. Assimakopoulos([1]), C. Eleftheriadis([2]), S. Galanopoulos([3]), S. Harissopoulos([4]), K.G. Ioannides([1]), D. Karadimos([1]), D. Karamanis([1]), M. Kokkoris([3]), A. Lagoyannis([4]), C. Lamboudis([2]), C. Papachristodoulou([1]), C.T. Papadopoulos([3]), N. Patronis([3]), G. Perdikakis([3]), E. Savvidis([2]), V. Vlachoudis([5]), R. Vlastou([3])
and the n_TOF Collaboration

[1]The University of Ioannina, 451 10 Ioannina, Greece
[2]Aristotle University of Thessaloniki, Greece.
[3]National Technical University of Athens, Greece.
[4]N.C.S.R. "Demokritos", Athens, Greece.
[5]CERN

January 15, 2006

ABSTRACT

An experiment has been designed for the high-precision measurement of neutron-neutron interaction parameters through the interaction of the two neutrons in the final state of the reaction ^{2}H(n,np)n. The proposed experiment is to be carried out at the CERN nTOF facility in the incident neutron energy range between 30 and 75 MeV. A kinematically "complete" experiment is envisaged, in which the momenta of one neutron and the proton in the final state of the reaction will be measured in coincidence at specific angles of detection that enhance nn final-state interaction. The experiment will run parasitically with the target placed at 155 m downstream from the lead target with minimal modifications of the nTOF neutron tube without affecting work at the experimental area. Depending on the target used (CD_2 or liquid deuterium) the time needed for the total running time is estimated between 15 days and one month. Spectra will be collected simultaneously in 18 neutron incident energy bins of 2.5 MeV and nn interaction parameters will be extracted from a minimum chi-square comparison with simulated spectra.

The nTOF facility at CERN has been constructed with the aim of measuring neutron cross sections in a wide range of energies across the Periodic Table of Elements. However, even during the planning stages, the obvious comment was made that the most basic cross section, namely the n + n cross section, could not be measured due to the unavailability of a free neutron target. It has been long realised that the neutron-neutron (nn) cross section, or more generally the nn interaction, as a function of energy can be studied only through reactions with two neutrons in the final state, such as the reactions

$$\pi^+ + {}^2\mathrm{H} \rightarrow \mathrm{n} + \mathrm{n} + \gamma \qquad (1.1)$$

or

$$\mathrm{n} + {}^2\mathrm{H} \rightarrow \mathrm{n} + \mathrm{n} + \mathrm{p}. \qquad (1.2)$$

For low relative energies of two nucleons, it is usual to express their interaction through two parameters, namely the nucleon-nucleon scattering length a_{NN} and the effective range $r_{0\mathrm{NN}}$. Their precise measurement is of great importance in Nuclear Physics. The scattering length, in particular, is a very sensitive measure of the strength of the potential.

In the past, several experiments have been performed to derive the two parameters for all possible pairs of nucleons and all possible spin states for relative angular momentum $\ell = 0$. The results obtained for the np and pp parameters, which are today known with considerable accuracy from simple experiments involving the scattering of neutrons and protons by hydrogen, are summarised in Table 1. Several values of the nn interaction parameters, as obtained in recent experiments, are given in Table 2. The values given in these Tables show at first glance that the nuclear force can be considered as charge symmetric with good precision and, with lower precision, charge independent. The most sensitive and least ambiguous way to study a small departure from charge independence is to investigate further the neutron-neutron scattering parameters. It should be further noted that the nn scattering length and effective range cannot be deduced by electromagnetic correction on the data obtained from pp scattering, because these corrections depend upon the nature of the potential used, i.e. whether it contains a hard core, a soft core or is velocity dependent.

Early studies of the reaction in eq. (1.2) yielded values of a_{nn} which were mutually inconsistent. The reason for the discrepancy was due to the fact that most of these experiments involved the observation of only one of the three products in the final state (see, e.g., [Il 61, St 72, Ha 77]). Measurement of the energy spectrum of only one final state particle, does not allow separating the effects of the primary reaction mechanism from those of the final state interaction [Bo 69]. These difficulties can be largely overcome through kinematically complete experiments that measure in coincidence the momentum of two of the three outgoing particles.

Several kinematically complete experiments have been performed in the past with the aim to measure neutron–neutron scattering length via the reaction in eq. (1.2), but the low energies of the incident neutron employed for this purpose allowed the interference from the interaction of other possible pairs of outgoing particles. In 1974 McNaughton *et al*. [McN 75] used 130 MeV neutrons in the reaction of eq. (1.2) to extract the nn scattering length, but the incident neutron energy was determined with poor resolution. In the last three decades several experiments were done to determine the neutron low energy scattering parameters. In 1972 W. Zeitnitz *et al.* [Ze 72] by a three-body calculation with separable potentials gave a_{nn}= -14.5 ± 0.8 fm and r_{0nn} = 2.7 ± 0.5 fm. The same group, two years later published different results [Ze 74], deduced from a complete charge dependent calculation using exponential form factors, a_{nn} = -16.3 ± 1.0 fm and r_{0nn} = 2.13 ± 0.4).

In 1978, Y. Onel *et al.* [On 78], using measurements of p + d break-up, gave the value a_{nn} = - 13.3 ± 3.1 fm and, from the shape of the relative neutron energy, a_{nn} = -17.5 ± 4.0 fm. In 1979, J. Soukup *et al.* [So 79] assuming the best value of neutron – neutron scattering length (α_{nn} = -16.3 ± 0.6 fm) determined the effective range r_{0nn} = 2.9 ± 0.4 fm. At the same time, W. von Witsch *et al.* [Wi 79], using charge dependent three-body calculations with S-wave rank-one separable potentials and exponential form factors, deduced the nn scattering length as a_{nn} = -16.9 ± 0.6 fm and, through exact three-body calculations, the corresponding effective range [Wi 80], as r_{0nn} = 2.65 ± 0.18 fm. More recently, D. E. Gonzáles Trotter *et al.* [Go 99] analysed their data with rigorous three nucleon calculations to determine the singlet nn and np scattering lengths, with results a_{nn} = -18.7 ± 0.6 fm and a_{np} = -23.5 ± 0.8 fm. The most recent publication on this issue is by V. Hun *et a.l* [Hu 00]. At 25.3 MeV incident neutron energy the value of the nn scattering length from the absolute cross section obtained from the nn FSI peak was a_{nn} = -16.3 ± 0.4 fm while the relative cross section, normalised in the region of np quasi-free scattering gave a_{nn} = -16.1 ± 0.4 fm. Data were also obtained at 16.6 MeV, yielding a_{nn} = -16.2 ± 0.3 fm.

The nTOF facility at CERN provides an intense neutron source with good energy resolution in a wide band of neutron energies. It is therefore feasible to perform a kinematically complete experiment for the high accuracy measurement of the nn scattering length and effective range via the reaction in eq. (1.2), simultaneously at various incident neutron energies between 30 and 75 MeV. The proposed experiment aims to measure the energy of the outgoing proton and neutron in coincidence in such an experimental configuration that the nn FSI is dominant. Contributions from all other possible FSI pairs will also be taken into account in order to extract the values of a_{nn} and r_{0nn} with the highest possible accuracy.

2. Theory

Experimental difficulties in studying multi-particle reactions arise mainly from the large set of kinematic variables needed for the complete specification of the final state. Ignoring spin variables, the final state of a reaction with N particles in the exit channel has $3N$ degrees of freedom and a complete determination of this state involves the measurement of $3N$ scalar parameters, e.g. the N momenta of the outgoing particles. From the knowledge of the initial

state and by applying energy and momentum conservation, the number of independent parameters is readily reduced by 4. Thus, in a reaction of the form

$$a_1 + a_2 \rightarrow a_3 + a_4 + a_5 \tag{2.1}$$

with three particles in the final state the determination of five independent parameters is required. An obvious choice would be the momentum of one particle and the direction of emission of another. However, in practice, in an experiment on a reaction of the form in eq. (2.1) the momenta of two of the particles in the final state are measured and the consequent overdetermination of the kinematic variables is used in order to reduce background events.

In this Section we shall consider the ramifications due to the presence of three particles in the final state of eq. (2.1) both with regard to the kinematics and the transition probability for reaching the final state through the possible mechanisms of the reaction. We shall also give all the mathematical expressions needed for the assessment of the results to be obtained in the proposed experiment. In what follows, we shall adopt the convention that a "complete" experiment is being carried out, in which the momenta of particles a_3 and a_4 in eq. (2.1) are measured while particle a_5 escapes detection. The main emphasis of course will be on the reaction ^{2}H(n,np)n.

2.1 KINEMATICS OF THREE-PARTICLE REACTIONS

We shall examine the kinematics of the reaction in eq. (2.1) by assuming that an incident beam of particles a_1 is along the Z-axis, a_2 is the target nucleus at the origin of the co-ordinate system and particles a_3 and a_4 are detected at polar angles (Θ_3,Φ_3) and (Θ_4,Φ_4), respectively. Then it may be easily shown [As 76] that in the laboratory system the kinetic energies T_3 and T_4 of particles a_3 and a_4 will be solutions of the equation

$$Q = \left(1+\frac{m_3}{m_5}\right)T_3 + \left(1+\frac{m_4}{m_5}\right)T_4 - \left(1-\frac{m_1}{m_5}\right)T_1 - 2\cos\Theta_3\left[\left(\frac{m_1 m_3}{m_5^2}\right)T_1 T_3\right]^{1/2}$$

$$- 2\cos\Theta_4\left[\left(\frac{m_1 m_4}{m_5^2}\right)T_1 T_4\right]^{1/2} + 2\cos\Theta_{34}\left[\left(\frac{m_3 m_4}{m_5^2}\right)T_3 T_4\right]^{1/2} \tag{2.2}$$

in which

$$\cos\Theta_{34} = \cos\Theta_3\,\cos\Theta_4 + \sin\Theta_3\,\sin\Theta_4\,\cos(\Phi_3 - \Phi_4) \tag{2.3}$$

m_k are the masses of particles a_k, T_1 is the beam energy and Q is the Q-value of the reaction.

For a particular nuclear reaction of the form in eq. (2.1) and a fixed set of incident energy and angles of observation of the emitted particles, eq. (2.2) gives the geometrical locus of the expected contributions in a three-dimensional isometric representation of population vs. $f_1(T_3,T_4)$ and $f_2(T_3,T_4)$, where f_1 and f_2 are functions of the kinetic energies of the two detected

particles. The particular choice $f_1 = T_3^{1/2}$, $f_2 = T_4^{1/2}$ describes an ellipse in the f_1, f_2 plane for T_3 and T_4 satisfying eq. (2.2). The more frequent choice $f_1 = T_3$, $f_2 = T_4$ on the other hand gives a distorted ellipse. The kinematic locus for the reaction in eq. (1.2) is given in fig. 1.

There are many cases in which the reaction in eq. (2.1) does not proceed directly to the final state of three particles, but rather this state is reached through a sequential two-body decay. We shall denote such a process by

$$\begin{array}{l} a_1 + a_2 \rightarrow C_{34}^{*} + a_5 \\ \qquad\qquad\quad \hookrightarrow \; a_3 + a_4 \; \ldots \end{array} \tag{2.4}$$

where C_{34}^{*} is understood to represent any two-body interaction between particles a_3 and a_4, which is sufficiently long-lived to produce a state with definite quantum numbers. The three dots in eq. (2.4) represent all possible permutations of the indices. Contributions from such a sequential decay will still be included in the direct break-up kinematic locus given by the solution of eq. (2.2) as a result of the same overall energy-momentum conservation. However, the further constraints, imposed by the formation of the intermediate state C_{ij}^{*}, restrict these contributions to discrete points along the kinematic locus. The kinematics of a sequential process depend on whether the two observed particles interact or whether the interaction takes place between one of the observed particles and the particle escaping detection. The relevant non-relativistic equations for either case have been worked out elsewhere [As 76] and will not be repeated here. Furthermore, the interaction in the final state implied in eq. (2.4) will, in general, depend on the relative energy of the interacting particles. In analysing experimental results from a three-body reaction it is often desirable to determine the relative energy $E(ij)$, $i \neq j = 3, 4, 5$ of particles a_i and a_j, the interaction of which could be responsible for contributions at a particular point along the kinematic locus of the reaction. Expressions for the relative energy $E(ij)$ for a given set of observed kinetic energies T_1, T_2 are also derived in [As 76].

All kinematic relations given above are derived non-relativistically. However, in the proposed experiment at the nTOF facility, where high incident energies will be considered, the accuracy needed requires the use of relativistic expressions. The solution of the relativistic version of eq. (2.2) has been worked out in a convenient form by J. Kane (see reference in [Bo 69]) in terms of the momenta of the particles in the final state as

$$P_4 = \frac{-bc \pm \sqrt{b^2(c^2-1) - 4a^2 m_4^2}}{c^2 - 4a^2} \tag{2.5}$$

in which

$$
\begin{aligned}
a &= T_1 + m_1 + m_2 - T_3 - m_3 \\
b &= P_1^2 + P_3^2 - 2P_3P_1\cos\Theta_3 + m_5^2 - m_4^2 - a^2 \\
c &= 2P_3[\cos\Theta_3\cos\Theta_4 + \sin\Theta_3\sin\Theta_4\cos(\Phi_3 - \Phi_4)] - 2P_1\cos\Theta_4
\end{aligned}
\tag{2.6}
$$

and m_k, P_k and T_k are the masses, momenta and kinetic energies of particle k in units such that $\hbar = 1$.

The momentum of the undetected particle 5 is given by

$$
\mathbf{P_5} = \mathbf{P_1} - \mathbf{P_3} - \mathbf{P_4} \tag{2.7}
$$

and the total and kinetic energies of particle k by

$$
\begin{aligned}
E_k^2 &= P_k^2 + m_k^2 \\
T_k &= E_k - m_k .
\end{aligned}
\tag{2.8}
$$

It was determined that for the reaction in eq. (1.2) relativistic and non-relativistic calculations differed by more than 1% above 30 MeV incident neutron energy.

2.2 REACTION CROSS SECTION

The transition probability for a given reaction is given by

$$
W = \frac{2\pi}{\hbar}\left|\,\mathrm{H}\,\right|^2 \frac{d\rho}{dt} \tag{2.9}
$$

in which H is the perturbing Hamiltonian for the transition from the initial to the final state and $d\rho/dt$ is the density of the final states which are available to the reaction. In the event that $|H|^2$ has no strong energy dependence, as is expected for the direct break-up in eq. (1.2), the matrix element may be approximated by a constant and the reaction cross section is dominated by phase space.

For a kinematically complete experiment, the expression for the differential phase space PS, for finite solid angles of the detectors $\Delta\Omega_3$, $\Delta\Omega_4$ and finite energy channel widths ΔT_3, ΔT_4 has been derived by Boyd [Bo 69] (see also [Zu 67]) in a form particularly suitable for calculations of simulations of experimental spectra as

$$
PS = \frac{P_3P_4\Delta\Omega_3\Delta\Omega_4\Delta T_3}{1 + \dfrac{E_4}{E_5}\,\dfrac{\mathbf{P_4}\cdot\mathbf{P_5}}{\mathbf{P_4^2}}} \tag{2.10a}
$$

or

$$
PS = \frac{P_3P_4\Delta\Omega_3\Delta\Omega_4\Delta T_4}{1 + \dfrac{E_3}{E_5}\,\dfrac{\mathbf{P_3}\cdot\mathbf{P_5}}{\mathbf{P_3^2}}} \tag{2.10b}
$$

These expressions were used in the calculations for simulated experimental spectra in the absence of final-state interaction.

2.3 FINAL-STATE INTERACTION

The mechanism of the reaction in eq. (2.4), which proceeds to the final state of three particles via a sequential process, has been investigated by Watson [Wa 52]. In the Watson Final State Interaction (FSI) model it is assumed that the reaction may be described as a two-step process consisting of a primary interaction, followed by the interaction of two particles in the final state. This assumption is valid if the lifetime of the final-state two-particle system is sufficiently long for its decay not to be influenced by the presence of the third particle. Then, it may be shown [Go 64, Bo 69, As 70] that the differential cross section for a kinematically complete experiment may be cast in the form

$$\frac{d^4\sigma}{dT_3 dT_4 d\Omega_3 d\Omega_4} = N \times PI \times FSI \times PS \tag{2.11}$$

in which N is an overall normalisation factor, PI is a factor which describes the primary interaction, FSI is the enhancement of the cross section caused by pairs of particles in the final state and PS the phase space modulation given in eqs. (2.10).

It has been shown by many authors [Zu 65, Bo 69] that if the interacting particles in the final state are nucleons, the term FSI may be expressed in terms of two parameters characterising the spin state formed in the final state as

$$FSI = \frac{\left(\frac{1}{r_0} + \frac{1}{a} + \frac{1}{2} r_0 k^2\right)^2}{k^2 + \left(\frac{1}{a} + \frac{1}{2} r_0 k^2\right)^2} \tag{2.12}$$

where r_0 is the effective range and a the scattering length, which give the $\ell = 0$ energy dependence of the two-nucleon scattering cross section through the expression

$$\sigma = \frac{4\pi}{k^2 + \left(\frac{1}{a} + \frac{1}{2} r_0 k^2\right)^2}. \tag{2.13}$$

In all the expressions above, $k = P_{rel}/\hbar$ is the relative wave number of the interacting pair of nucleons in the particular spin state.

If we consider a kinematically complete experiment in which particle a_3 is a neutron and particle a_4 is the proton, then, for relative angular momentum $\ell = 0$, the possible two nucleon states in the reaction of eq. (1.2) are schematically depicted in Fig. 2. We note that the figure

further distinguishes whether the interaction is between the two detected particles or a detected particle and the particle escaping detection. All these interactions are expected to contribute to the cross section at points along the kinematic locus of Fig. 1 where, according to eq. (2.12), the relative momentum of the interacting pair is small. We may thus write the *FSI* term in eq. (2.11) as the sum

$$FSI = C_{34}^{S}E_{34}^{S} + C_{45}^{S}E_{45}^{S} + C_{34}^{T}E_{34}^{T} + C_{45}^{T}E_{45}^{T} + C_{35}^{S}E_{35}^{S} \tag{2.14}$$

in which C_{ij}^{k} represents the probability that the primary interaction leaves nucleons *i* and *j* in the spin state *k* and

$$E_{ij}^{k} = \left|\Psi^{k}(i,j)\right|^{2} \tag{2.15}$$

is the corresponding enhancement in the cross section due to the final state interaction as given by eq. (2.12). In eq. (2.15), $\Psi^{k}(i,j)$ is the amplitude for the primary reaction leaving particles *i* and *j* in spin state *k*.

Eq (2.14) may be further simplified if we make the assumption that the two virtual deuteron states are produced with the same probability at the primary interaction of eq. (1.2). Setting

$$\begin{aligned} C_{34}^{S} &= C_{45}^{S} \\ C_{34}^{T} &= C_{45}^{T} \end{aligned} \tag{2.16a}$$

$$\frac{C_{34}^{T}}{C_{34}^{S}} = \frac{C_{45}^{T}}{C_{45}^{S}} = R \tag{2.16b}$$

and for simplicity of the symbolism $C_{nn} = C_{35}^{S}$, eq. (2.14) becomes

$$FSI = E_{34}^{S} + E_{45}^{S} + R(E_{34}^{T} + E_{45}^{T}) + C_{nn}E_{35}^{S}\,. \tag{2.17}$$

2.4 THE PRIMARY INTERACTION

If the reaction ^{2}H(n,np)n proceeds to the final state exclusively through the sequential process just described, then the primary interaction factor *PI* in eq. (2.11) may be taken as a constant and in fact, due to the inclusion of the overall normalisation term *N*, equal to 1. However, if other primary reaction mechanisms are possible, they must be taken into account in the calculation of *PI*.

One mechanism that has been described in the literature and may affect the primary interaction is the "spectator" effect, which refers to the case of the incident neutron interacting with only one nucleon in the deuteron, e.g. the proton. Then, the target neutron participates in the overall process as a simple "spectator". This process may be treated in the framework of a

simple knockout model using the Born approximation [Ph 64, Zu 65]. Assuming a Hulthén type wave function for the deuteron, the amplitude for this process is [Do 64]

$$\left|\Psi(P_n)\right|^2 = \frac{1}{P_n^2+\alpha^2} - \frac{1}{P_n^2+\beta^2} \tag{2.18}$$

in which P_n is the momentum transferred to the spectator neutron in the target, $\alpha = -m_n B$ and $\beta = 7\alpha$; B = - 2.226 MeV and m_n are the deuteron binding energy and the neutron mass, respectively. If C_S is the strength of the spectator effect, then the primary interaction term should be modified to

$$PI = (1 - C_S) + C_S \left|\Psi(P_n\right|^2 . \tag{2.19}$$

Another factor that may affect the primary production mechanism is due to the interference of matrix elements arising from processes that cannot be experimentally distinguished. Since the spins of the three outgoing particles could be in principle measured, a neutron with spin up is distinguishable from a neutron with spin down. Therefore, final states with different spins should be considered as distinguishable and their amplitudes should add incoherently as in the case of eq. (2.14). In fact, the only indistinguishable diagrams in Fig. 2 are the singlet nn and the singlet np final state interactions and the corresponding amplitudes $\Psi^S(n,n)$ and $\Psi^S(n,p)$ should add coherently in the calculation of the term *FSI*. It may be shown [Bo 69] that the effect of this is to modify eq. (2.17) as

$$FSI = E_{34}^S + E_{45}^S + R(E_{34}^T + E_{45}^T) + C_{nn}(1 + C_{in}k_{nn})E_{35}^S \tag{2.20}$$

in which k_{nn} is the relative wave number of the two outgoing neutrons and C_{nn} a constant. Eqs. (2.19) and (2.20) are the final expression, which will be used in the evaluation of the spectra expected in the experiment proposed here.

The Watson final-state interaction theory has met with considerable success in the analysis of experiments on reactions with three particles in the final state [Do 64, Bo 69, As 70]. Indeed, the main aim of the experiment performed on the ^{2}H(p,pp)n reaction by Boyd, *et al.* [Bo 69] was to verify that the correct scattering length and effective range for the np interaction, accurately known from ^{1}H(n,p)n cross section measurements, could be obtained through the study of final-state two-nucleon interaction. It is expected that the Watson model will be more successful as the centre of mass energy – and hence the relative velocity – between a nucleon and an interacting pair of nucleons in the final state gets higher. In the p + ^{2}H experiment of Boyd, *et al*. [Bo 69] the centre of mass energy between the proton and the interacting np singlet state was limited by the maximum energy of the accelerator to 8.5 MeV. In the proposed n + ^{2}H experiment at the nTOF facility, in the range of 30 to 75 MeV incident neutron energy, the corresponding centre of mass energy between the di-neutron and the receding proton in the final state will be between 18 and 47 MeV. This is one of the reasons for which the nTOF facility is admirably suited for carrying out the proposed experiment.

3. Experimental considerations

The experimental set-up for the proposed experiment is given schematically in Fig. 3. Two detectors D3 and D4 are placed at angles* ($\Theta_3 = 34°$, $\Phi_3 = 0°$) and ($\Theta_4 = 80°$, $\Phi_4 = 180°$) with respect to the neutron beam for the detection of one neutron and the proton, respectively, in the final state of the reaction

$$n + {}^2H \rightarrow n + p + n \qquad (3.1)$$

In this geometry, the experiment detects only co-planar events – or almost co-planar if the finite extent of the detector collimators is taken into account.

It is envisaged that the target will be placed at 155 m (Fig. 4) downstream from the lead target, instead of the experimental area at 182.5 m, because the neutron flux in the experimental area of the nTOF facility is not sufficiently high to ensure an acceptable counting rate. At 155 m, the charged particles have already been removed by the sweeping magnet [nT 00] and the neutron flux is greater due to the absence of the last collimator and the effect of the $1/r^2$ law. In this fashion, the experiment could run parasitically, while other measurements are performed in the experimental area.

Each component of the experimental set-up is discussed in some detail below.

3.1 THE NEUTRON BEAM

An estimate of the neutron flux at 155 m from the lead target is based on the given flux obtained [nT 00] at the experimental area (187.5 m). From the simulated energy distribution of the neutrons, for a proton pulse of 7×10^{12} protons, it is deduced that in the energy bin of 50 to 52.5 MeV, only 780 neutrons/(cm^2·bunch) reach the experimental area. It is foreseen that one bunch every 2.4 s will be available for the nTOF facility. The flux at 155 m is increased by a factor of 7 due the absence of the last collimator; an enhancement in neutron flux due the $1/r^2$ law is also expect. According to these corrections, the expected neutron flux at 155 m with energies in the interval 50 - 52.5 MeV is equal to 3.3×10^3 n s^{-1} cm^{-2}. This estimate is not expected to vary drastically for 2.5 MeV energy bins in the range 30 – 75 MeV.

3.2 TARGETS

Two types of targets are being considered:

1. A liquid deuterium target with thin aluminium windows.
2. A self-supported CD_2 target.

The main limitation on target thickness comes from the energy loss of the outgoing pro-

* For the particular choice of angles, see below Section 3.4

ton while it traverses the target. In the case of a liquid deuterium target the energy loss in the aluminium window must also be taken into account. To minimise energy loss effects, the target will be tilted towards the proton detector at an angle $\Theta_T = \Theta_4$ (= 80°). If the tolerance for maximum energy loss of a 10 MeV proton is set at 2 MeV and an aluminium window for the liquid deuterium target of thickness 10 μm is assumed, then the maximum thickness of the liquid deuterium target is 1800 μm and for the CD_2 target 400 μm.

The amount of ^{2}H nuclei available for the reaction in eq. (3.1) differs for each target. It may be easily calculated that for the thickness mentioned above, the liquid deuterium target, when placed vertically to the neutron beam, presents 9.1×10^{21} ^{2}H nuclei cm^{-2}; the corresponding number for the CD_2 target is 3.2×10^{21} ^{2}H nuclei cm^{-2}. Thus, the liquid ^{2}H target has a clear advantage over CD_2 by almost a factor of 3. It is also noted that the CD_2 target will cause contamination of the experimental data from the reaction $^{12}C(n,np)^{11}B$, although such events could be easily sorted out from kinematics considerations.

By tilting the target by an angle of $\Theta_T = 80°$, the density of ^{2}H nuclei available to the reaction increases by a factor of $1/\cos\Theta_T = 5.76$. In order to avoid inordinate smearing out of the spectra due to the uncertainty of the reaction position on the target, the shape of the target will be that of an ellipse with its long axis equal to 22.9 cm and the short axis equal to 4 cm. In this geometry, the profile of the target presented to the neutron beam will be a disk with a diameter of 4 cm.

If the proposed experiment is to be run in a parasitic mode, then the effect of the presence of the target at 155 m on the neutron beam of the nTOF facility must be investigated. For this purpose, extensive GEANT4 simulations were performed. In these simulations, a neutron beam of 4 cm diameter was assumed to hit the target and the energy spectrum of the neutrons escaping the target was monitored in a virtual detector placed along the beam axis. As shown in Fig. 5, the beam is not seriously affected at neutron energies above 4 MeV Below 4 MeV, the simulations showed that only a few percent of the neutrons that traverse the target lose the proper TOF-energy relationship. It is thus concluded that the effect of the deuteron target on the neutrons that cross the second collimator and end up in the experimental area will be negligible.

3.3 DETECTORS

The neutrons emitted from the reaction in eq. (3.1) will be detected by a NE213 liquid scintillator, with dimensions 12.7 cm in diameter and 12.7 cm thickness, coupled to a fast photomultiplier tube. This detector has been extensively used in experiments involving neutrons [Wi 79, St 89, Ba 95] and provides fast time response, good n/γ discrimination, and high efficiency. The time response of the detector, which is a crucial factor in TOF measurements, is less than 1 ns [Me 99]. Good n/γ discrimination is also required due to the strong gamma background present in all neutron experiments. At the nTOF facility at CERN, a Flash ADC acquisition system is used, thus particle identification will be performed according to ref. [Ma 01].

The efficiency of the NE213 detector is strongly depended on the threshold level. For Am-Be bias (4.439 MeV-4.331 MeV) the efficiency of the detector for neutron energies related to the proposed experiment is about 12% [Me 97, No 01]. A higher efficiency could be attained by increasing the thickness of the detector, but this would also increase the uncertainty in the emitted neutron path length.

Due to the large dynamic energy range of the protons emitted in the reaction of eq. (3.1), they will be detected with a triple Si surface-barrier detector telescope. The optimum combination of thickness of each detector in the telescope was determined as $\Delta E_1 = 35$ μm, $\Delta E_2 = 565$ μm and E = 7.4 mm. The active area of the telescope (collimator dimensions) will be 1.5 × 5 cm. With these dimensions protons with energies from 2 MeV up to 39 MeV can be detected and identified against elastic scattered deuterons and alpha particles.

The time response of the proton detector is crucial for this experiment because it determines the start signal of the TOF of the emitted neutron or the stop signal of the TOF of the incident neutron. For this reason, the Si detectors would be probably cooled to about – 50 °C. Time signals from the proton telescope will be derived from the ΔE_1 detector with the aim of achieving a time resolution of less than 0.5 ns.

3.4 CHOICE OF ANGLES, DETECTOR DISTANCES AND DETECTOR COLLIMATORS

Since the main aim of the proposed experiment is the observation of the nn final-state interaction, the angles of detection in Fig. 3 must be such that the two neutrons are emitted from the primary interaction with low relative momentum. To determine such a pair of angles, the reaction in eq. (3.1) may be treated as a two-body reaction with a Q-value equal to the binding energy of the deuteron and the virtual di-neutron treated as one particle of mass $2m_n$, i.e.

$$n + {}^2H \rightarrow (nn) + p, \qquad Q = -2.226 \text{ MeV}. \tag{3.2}$$

Evidently, the choice of an angle Θ_3 for the emission of the di-neutron, will result in a single value of the angle Θ_4 for the emission of the proton. Several such pairs of angles were examined. The particular set of angles $\Theta_3 = \Theta_n = 34°$ and $\Theta_4 = \Theta_p = 80°$, finally selected for the performance of the proposed experiment, ensures in addition that the energies of both the detected particles are relatively large and comparable. From the examination of kinematics for this choices of angles, it also emerges that the relative momenta of the two other pairs of nucleons in the final state are large, so that no interference from other FSI resonances are expected in the region of interest. The kinematic locus for this choice of angles is contained in Fig. 6.

Detector distances and collimator sizes were chosen through the following considerations:

- Dimensions of readily available detectors for neutrons (NE213) and protons (surface barrier detectors).

- A reasonable TOF path for the outgoing neutron, with minimum modifications needed

in the nTOF tunnel.

- Reasonable solid angles subtended by the detectors (of the order of 10^{-3} sr).

3.5 DATA ACQUISITION

Signals from all detectors (NE213, ΔE_1, ΔE_2 and ΔE) will be recorded by flash ADCs. The off-line analysis for the identification of a valid event from the reaction in eq. (3.1) will follow the following steps:

1. A coincidence check will be performed between NE213 and ΔE_1 and the time of arrival of the two particles t_3 and t_4 will be recorded.

2. For successful events in step 1, a coincidence check will be performed for detectors ΔE_1, ΔE_2 and ΔE of the charged-particle telescope. Mass identification will be performed and the total kinetic energy T_4 of the detected particle will be calculated.

3. If the particle detected in Step 2 is a proton, the instant t_1 that the reaction in eq. (3.1) occurred will be calculated from t_4 and the kinetic energy T_4 of the particle.

4. From the time of flight $t_3 - t_1$, the energy of the neutron detected in NE213 will be computed.

5. The instant t_1 will also give the energy T_1 of the incident neutron that caused the reaction in eq. (3.1).

Events will be stored in three-dimensional spectra of population versus $T_3 \times T_4$, each representing an energy bin ΔT_1 of the incident neutron energy T_1 (e.g., $\Delta T_1 = 2.5$ MeV). Examples of the spectra expected in the proposed experiment are presented by the simulations in Section 4 below.

3.6 COUNTING RATES

The expected counting rate from the reaction in eq. (3.1) may be estimated by the incident neutron flux, the number of target nuclei per cm^2 presented to the beam and the reaction cross section. The first two quantities are well known. However, in order to calculate the expected counting rate, an estimate of the cross section has to be made.

All experiments performed to date have demonstrated that the reaction in eq. (3.1) proceeds to the final state primarily through final-state interaction of a pair of the outgoing particles, with direct break-up into three independent particles (phase space) constituting only about 10 % of the primary interaction cross section. In terms of eq. (2.11) this means that the term *FSI* is strongly modulated, with most of the cross section residing in nn or np resonances. Thus, since the geometry of the experiment has been chosen so that it resides on one of these resonances, it is expected to capture a large part of the primary interaction cross sec-

tion and we may write the expected counting rate W (events per second) as

$$W = I(n) N_T \sigma' \tag{3.3}$$

in which $I(n)$ is the incident neutron flux (n s^{-1} cm^{-2}), N_T is the number of target nuclei exposed to the beam* and σ' is a substantial part (e.g., 50 %) of the primary interaction cross section.

Data for incident neutron energies up to 20 MeV are available from the ENDFB-VI database. The estimation of the primary interaction cross section was drawn from data of d(p, p)pn experiments [As 76b], for which no great differences from the d(n,n)np cross section are expected. The average value deduced from these data, for incident neutron energies between 30 and 75 MeV, was in the range of 0.1 – 0.3 mbarn, with a tendency to increase at low energies. We have therefore adopted the token value of 0.1 mbarn for the estimation of the counting rate in eq. (3.3).

The values of the quantities $I(n)$ and N_T have already been given above as

$$\begin{aligned} &I(n) = 3.3 \times 10^3 \quad \text{n s}^{-1}\ \text{cm}^{-2} \\ &N_T(\text{CD}_2) = 3.2 \times 10^{21} \quad {}^2\text{H nuclei cm}^{-2} \\ &N_T(\text{liquid } {}^2\text{H}) = 9.1 \times 10^{21} \quad {}^2\text{H nuclei cm}^{-2}. \end{aligned} \tag{3.4}$$

In the convention adopted here, the values for N_T have to be multiplied by the area of the target (4π cm^2) and divided by the cosine of the target angle Θ_T (= 80°). The values for N_T thus become

$$\begin{aligned} &N_T(\text{CD}_2) = 2.3 \times 10^{23} \quad {}^2\text{H nuclei} \\ &N_T(\text{liquid } {}^2\text{H}) = 6.58 \times 10^{23} \quad {}^2\text{H nuclei} \end{aligned} \tag{3.5}$$

so that the estimate for the counting rate in eq. (3.3) becomes

$$\begin{aligned} &W(\text{CD}_2) = 0.1 \cdot 3.3 \times 10^3 \cdot 2.3 \times 10^{23} \cdot 0.1 \times 10^{-27} = 0.008 \text{ cps} \\ \text{or} \\ &W(\text{liquid } {}^2\text{H}) = 0.1 \cdot 3.3 \times 10^3 \cdot 6.58 \times 10^{23} \cdot 0.1 \times 10^{-27} = 0.02 \text{ cps} \end{aligned} \tag{3.6}$$

where the leading factor of 0.1 is due to the efficiency of the NE213 detector. This is equivalent to a counting rate in every $\Delta T_1 = 2.5$ MeV bin spectrum of about 700 events per day for a CD_2 target or 1900 events per day for a liquid ^2H target. Hence, for the accumulation of 10,000 events in each spectrum, a real-time running period of about 15 days will be required in the first case and about 5.5 days in the second.

* It is noted that in experiments involving charged particle beams, the incident flux I is usually expressed in [particles s^{-1}] and the target nuclei density N_T in [nuclei cm^{-2}]. The different choice made in eq. (3.3) is due to

4. Simulation of experimental spectra

In realistic experimental conditions, the finite extent of the target and the detector collimators tend to smear out the kinematic locus in Fig. 6. This effect is enhanced by the energy loss of the proton in the target and the resolution of the detectors.

In order to assess the spectra expected from the proposed experiment, a computer code was written (in Visual Basic) to simulate experimental conditions. This is a Monte Carlo calculation which considers successive events according to the following steps:

1. The experimental set-up in Fig. 3 is assumed with the neutron beam along the positive direction of the Z-axis and two detectors placed with their planes perpendicular to the XZ-plane with the centre of their collimators at points defined by the angles (Θ_3, Φ_3 = 0°) for the neutron and (Θ_4, Φ_4 = 180°) for the proton detector; the detector collimators can be either circular or rectangular.

2. A random point (x_T, y_T, z_T) within the active volume of the target and two random points on the surface of the two detectors are selected. For these points, the corresponding angles (Θ_3', Φ_3') and (Θ_4', Φ_4') of emission of the neutron and the proton, respectively, are calculated.

3. Kinematic variables (kinetic energy, momentum, relative momenta, etc.) for the angles (Θ_3', Φ_3') and (Θ_4', Φ_4') are calculated and the corresponding contributions to phase space and the cross section in eq. (2.11) for each of the *FSI* terms in eq. (2.17) are computed. These contributions are added, each to a separate 64×64 spectrum array. Finally, the separate spectra for the contribution from each separate FSI interaction are added to form the simulated experimental spectrum.

4. Since each simulated spectrum is to represent a finite range ΔT_1 of incident neutron energies, the previous process is repeated for ten discrete steps across a pre-selected range ΔT_1.

5. In order to take into account the energy loss of the proton in the target, the path length of the proton inside the target is calculated from the geometry of the event and an amount ΔT_4, calculated according to Ziegler's stopping power theory, is subtracted from its kinetic energy T_4 before placing its contribution into the 64×64 spectrum array.

6. Finally, the finite resolution of the detectors is taken into account by smearing out each point in the simulated spectra according to a Gaussian with FWHM equal to the resolution of each detector.

---

the large profile of the neutron beam and the smaller extent of the target. With either definition, the product IN_T has the same numerical value.

From the FSI theory described in Section 2, it follows that the simulated spectra will depend on the values of 7 parameters, namely

N	the overall normalisation factor
C_{nn}	the strength of the nn final-state interaction
R	the relative strength of triplet-to-singlet np final-state interaction
C_S	the relative strength of the spectator effect
C_{in}	the contribution of interference terms
a_{nn}	the scattering length of the (singlet) nn interaction
r_{0nn}	the effective range of the (singlet) nn interaction

Four more parameters, namely the scattering length and effective range of the np interaction in the singlet and triplet states, could be added to this list. However, for the purposes of the proposed experiment, the values of these parameters are considered known with sufficient accuracy and are set according to the data in Table 1. In addition, the geometry and the energies involved in the proposed experiment warrant the setting of $C_S = C_{in} = 0$.

The front-end screen of the simulation code, where all parameters pertaining to the geometry of the experiment and the theory are defined, is contained in Fig. 7. The output of the code is

1. A file containing the simulation ID (see Fig 7)

2. A file containing the kinematic locus of the reaction in the $T_3 \times T_4$ plane (see Fig. 8)

3. One file containing the phase space cross section for direct three-body break-up (see Fig. 9)

4. Five files containing the separate contributions of each term in eq. (2.17)

5. One file containing the expected spectrum (see Fig. 10).

The values of parameters pertaining to the nn interaction will be extracted from the comparison of simulated with experimental spectra. In this context it is interesting to examine the sensitivity of the data with regard to variations of the nn scattering length and effective interaction. Thus, the dependence of the shape of the simulated spectra on the parameters on p. 15 has been thoroughly investigated in order to determine the sensitivity with which the nn interaction parameters can be extracted from the proposed experiment. An example which shows drastic changes in the shape of the expected spectra that a variation of 1 fm in the value of a_{nn} causes in the simulated spectrum is contained in Fig. 11.

It is envisaged that the nn interaction parameters will be extracted through a minimum chi-square comparison (e.g., through the CERN library code MINUIT [Ja 75]) of simulated and experimental spectra. For this reason the simulation code has been translated into FOR-

TRAN and has been incorporated into MINUIT's Subroutine FCN. To test this procedure, pseudo-data were constructed by adding to each point of the spectrum of Fig. 10(b) an "experimental" error of two standard deviations, suitably randomised through the expression

$$\sigma = 2\,R(-1,1)\sqrt{N} \tag{4.1}$$

in which N is the number of counts in the spectrum channel and R(-1,1) a random number between –1 and 1. The pseudo-data constructed in this manner are shown in Fig. 12(a). By employing these data, MINUIT was made to perform a search with starting values of the parameters far from the ones assumed for the construction of the data. The results of one such search are contained in Fig. 12(b).

5. Conclusions

The investigation of the feasibility of a kinematically complete experiment on the ^{2}H(n,np)n reaction at the nTOF facility of CERN with the aim of obtaining accurate values of the neutron-neutron interaction parameters has shown that the proposed research can be conducted with a high degree of confidence for the attainment of its goals. The experiment can be run parasitically at 155 m downstream from the lead target with small modifications of the nTOF neutron tube without affecting work at the target area. Depending on the target used (CD_2 or liquid deuterium) the time needed for the execution of the experiment is between 15 days and one month. Spectra will be collected simultaneously in 18 neutron incident energy bins of 2.5 MeV width in the range of 30 to 75 MeV. The accumulation of data in such a large dynamic range is expected to further increase the precision in the measurement of the nn interaction parameters.

References

Ar 74 R.A.Arng, R.H. Hackman and L.D. Roper, Phys. Rev. **C9** (1974) 555

As 70 P.A. Assimakopoulos, E. Beardsworth, D.P. Boyd and P.F. Donovan, Coincidence studies of the reactions $^{3}He + {}^{2}H$ and $^{4}He + {}^{2}H$, Nucl. Phys. **A144** (1970) 272-288

As 76 P.A. Assimakopoulos, Kinematics of three-body reactions, Comp. Phys. Comm. **10** (1976) 385-400

As 76b Asoke N. Mitra, Ivo Slaus, V. S. Bhasin, V. K. Gupta, *Few Body Dynamics*, Proceedings of the VII International Conference in Nuclear and Particle Physics, North Holland Publishing Company, 1976, pp 193, 201 and 213

Ba 95 J. Balewski, K. Bodek, L. Jarczyk, B. Kamys, St Kirstyn, A. Strzałkowski, W. Hajdas, R. Müller, B. Dechant, J. Krug, W. Lübcke, H. Rühl, G. Spangardt, M. Steinke, M. Stephan, D. Kamke, R. Henneck, H. Witała, W. Glöcke, and J. Golak, Nucl. Phys. **A581** (1995) 131

Bo 69 D.P. Boyd, P.F. Donovan and J.F. Mollenauer, Proton-neutron final-state interaction, Phys. Rev. **188** (1969) 1544-1567

Di 75 W. Dilg, Phys. Rev. **C11** (1975) 103

Do 64 P.F. Donovan, J.V. Kane, Č. Zupančič, C.P. Baker and J.F. Mollenauer, Phys. Rev. **135** (1964) B75

Go 99 D. E. Gonzales Trotter, F. Salinas, Q. Chen, A. S. Crowell, W. Glöckle, C. R. Howell, C. D. Roper, D. Schmidt, J. Slaus, H. Tang, W. Tornow, R. L. Walter, H. Witała, and Z. Zhou, Phys. Rev. Lett **83** (1999) 3788

Ha 77 R. C. Haight, S. M. Grimes, and D. Anderson, Phys. Rev. **C16** (1977) 97

Hu 00 V.Huhn, L. Wätzold, Ch. Weber, A. Siepe, W. von Witsch, H. Witala, and W. Glöckle, Phys. Rev. **C63**, (2000) 014003

Il 61 K. Ilakovac, L. G. Kuo, M. Petravić, and I. Šlaus, Phys. Rev. **124 (**1961) 1923

Ja 75 F. James and M. Ross, MINUIT – A system of function minimization and analysis of the parameter errors and correlations, Comp.Phys. Com. **10** (1975) 343

Ko 75 L. Koester, and W. Nistler, Z. Phys. **A272** (1975) 189

Kr 88 K.S. Krane, *Introductory Nuclear Physics*, John Wiley & Sons, 1988

Ma 84 L. Mathelitsch, B.J. VerWest, Phys. Rev. **C29** (1984) 739

Ma 01 S. Marrone, D. Cano-Ott, N. Colonna, F. Gramegna, F. Gunsing, M. Heil, F. Käppeler, P.F. Mastinu, P.M. Milazzo, T. Papaevangelou, P. Pavlopoulos, R. Plag, R. Reifarth, G. Tagliente, J. L. Tain, K. Wisshak, "Analysis of liquid scintillator pulse shape for neutron studies", Preprint submitted to Elsevier Preprint, 18/1/2001

McN 75 M. W. McNaughton , R. J. Griffiths, I. M. Blair, B. E. Bonner, J. A. Edgington, M. P. May, and N. M. Stewart, Nucl. Phys. **A239** (1975) 29

Me 99 S. Meigo, H. Takada, S. Chiba, T. Nakamoto, K. Ishibashi, N. Matsufuji, K. Maehata, N. Shigyo, Y. Watanabe, and M. Numajiri, Nucl. Instr. and Meth. in Phys. Res. **A431** (1999) 521

Me 97 S. Meigo, Nucl. Instr. and Meth. in Phys. Res., **A401** (1997) 365

Na 01 Noriaki Nakao, Tadahiro Kurosawa, Takashi Nakamura, and Yoshitomo Uwamino, Nucl. Instr. and Meth. in Phys. Res., **A463** (2001) 275

nT 00 The nTOF Collaboration Technical Report, CERN/INTC 2000-018,3/11/2000

Ph 64 R.J.N. Phillips, Nucl. Phys. **53** (1964) 650

So 79 J. Soukup, J. M. Cameron, H. W. Fielding, A. H. Hussein, S. T. Lam, and G. C. Neilson

St 72 A. Stricker, Y. Saji, Y. Ishizaki, J. Kokame, H. Ogata, T. Suehiro, I. Nonaka, Y. Sugiyama, S. Shirato, and N. Koori, Nucl. Phys. **A190** (1972) 284

St 79 M. Stephan, K. Bodek, J. Krug, W. Lübcke, S. Obermanns, H. Rühl, M. Steinke, D. Kamke, H. Witała, Th. Cornelius, and W. Glöckle, Phys. Rev. **C39** (1989) 2133

Wa 52 Kenneth M. Watson, Physical Review, **88** (1952) 1163

Wi 79 W. von Witsch, B. Gómez Moreno, W. Rosenstock, K. Ettling, and J. Bruinsma,

Nucl. Phys. **A329** (1979) 141

Wi 80 W. von Witsch, B. Gómez Moreno, W. Rosenstock, R. Franke, and B. Steinheuer, Nucl. Phys. **A346** (1980) 117

Ze 72 B. Zeitnitz, R. Maschuw, P. Suhr, and W. Ebenhöh, Phys. Rev. Lett. **19** (1972) 1656

Ze 74 B. Zeitnitz, R. Maschuw, P. Suhr, W. Ebenhöh, J. Bruinsma, and J. H. Stuivenberg, Nucl. Phys. **A231** (1974) 13

Zu 65 Č. Zupančič, Rev. Mod. Phys. **37** (1965) 332

Zu 67 Č. Zupančič, Simple aspects of three-particle reactions in nuclear physics, in *Les réactions nucléaires à trois corps*, IX^{e} cours de perfectionnement, Association vaudoise des chercheurs en physique et le laboratoire de physique nucléaire de l' Université de Grenoble, Zermatt, 2 – 8 April, 1967

TABLES

Table 1. pp and np scattering parameters.

Parameter	Value(fm)	Reference
a_{pp}	-7.822 ± 0.003	Ma 84
r_{0pp}	2.775 ± 0.006	Ma 84
a_{np}(singlet)	-23.748 ± 0.009	Ko 75
r_{0np} (singlet)	2.77 ± 0.05	Di 75
a_{np}(triplet)	5.423 ± 0.004	Di 75
r_{0np}(triplet)	1.760 ± 0.005	Di 75

Table 2. nn scattering parameters.

a_{nn} (fm)	r_{0nn} (fm)	Reference
-14.5 ± 0.8	2.7 ± 0.5	Ze72
-16.3 ± 1.0	2.13 ± 0.4	Ze 74
-13.3 ± 3.1		On 78
-17.5 ± 4.0		On 78
	2.9 ± 0.4	So 79
-16.9 ± 0.6		Wi 79
	2.65 ± 0.18	Wi 80
-18.7 ± 0.6		Go 99
-16.3 ± 0.4		Hu 00
-16.1 ± 0.4		Hu 00
-16.2 ± 0.3		Hu 00

Figure captions

Figure 1. Kinematic locus for the reaction

$$n + {}^2H \rightarrow n + p + n$$

at incident energy E_n = 50 MeV. The neutron and proton are detected at angles $\Theta_n = 20^o$, $\Phi_n = 0^o$ and $\Theta_p = 50^o$, $\Phi_p = 180^o$, respectively.

Figure 2. Representation of possible final state interaction diagrams, The primary interaction is represented with large circles and the final-state interaction with small circles. The arrows on the right correspond to various spin states of the interacting nucleons.

Figure 3. Schematic experimental setup for the proposed experiment.

Figure 4. The position of the deuterium target in the proposed experiment in the nTOF beam tube.

Figure 5. Energy spectra of neutrons hitting the virtual detector in the absence of target (red line) and after a CD_2 or liquid D_2 target is placed in the neutron beam (black line).

Figure 6. Kinematic locus for the reaction

$$n + {}^2H \rightarrow n + p + n$$

at incident energy E_n = 50 MeV. The neutron and proton are detected at angles $\Theta_n = 35.5^o$, $\Phi_n = 0^o$ and $\Theta_p = 80^o$, $\Phi_p = 180^o$, respectively.

Figure 7. The front-end screen of the simulation code.

Figure 8. The output file with the job ID for the screen in Fig. 7.

Figure 9. (a) Broadening of the kinematic locus in Fig. 6 due to the effect of finite beam size and extend of the detector collimators. Events involving outgoing particles with kinetic energy less than 5 MeV have been eliminated. (b) Projection of the kinematic locus onto the $T_3 \times T_4$ plane of the simulated spectrum with parameters defined in Fig. 8.

Figure 10. Simulated spectra for the parameters in Fig. 8. (a) Phase space from the direct three-body break-up. (b) Total spectrum around the nn FSI resonance.

Figure 11. Comparison of two simulated spectra created for a difference of 1 fm in the value of the nn scattering length.

Figure 12. (a) Pseudo-data obtained by adding two randomised standard deviations to the simulation spectrum of Fig. 11 (a_{nn} = - 16.1 fm); effective range r_{0nn} = 3.2 fm. (b) Result of MINUIT minimum chi-square search; $\chi^2 = 1.516$, a_{nn} = - 16.18 fm, r_{0nn} = 3.21 fm.

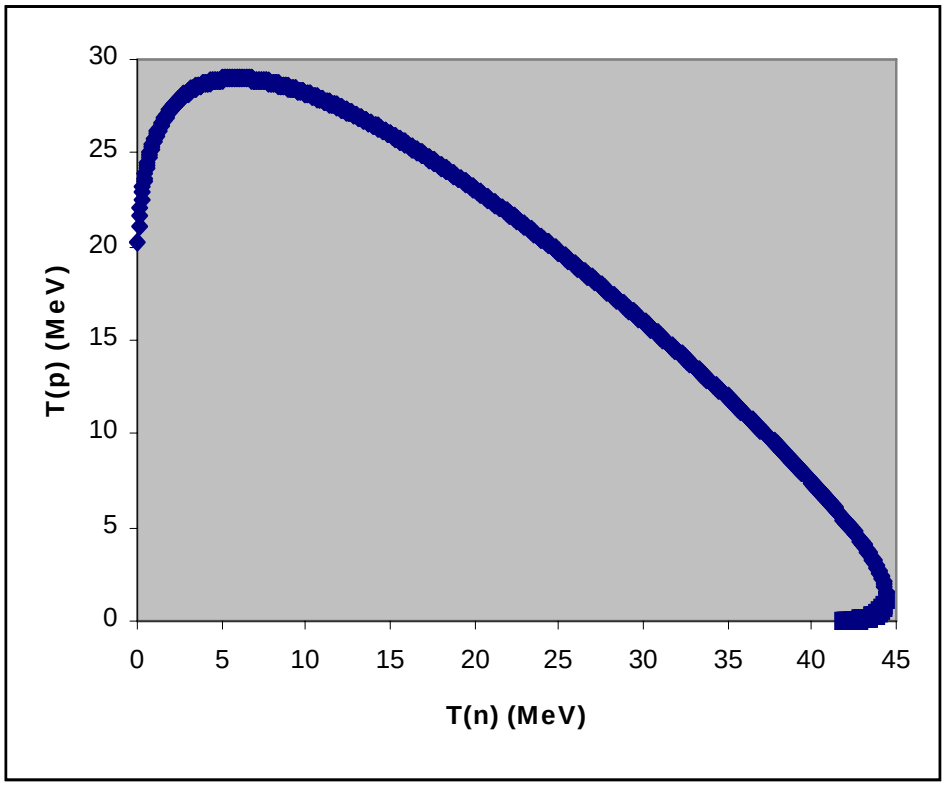

FIGURE 1

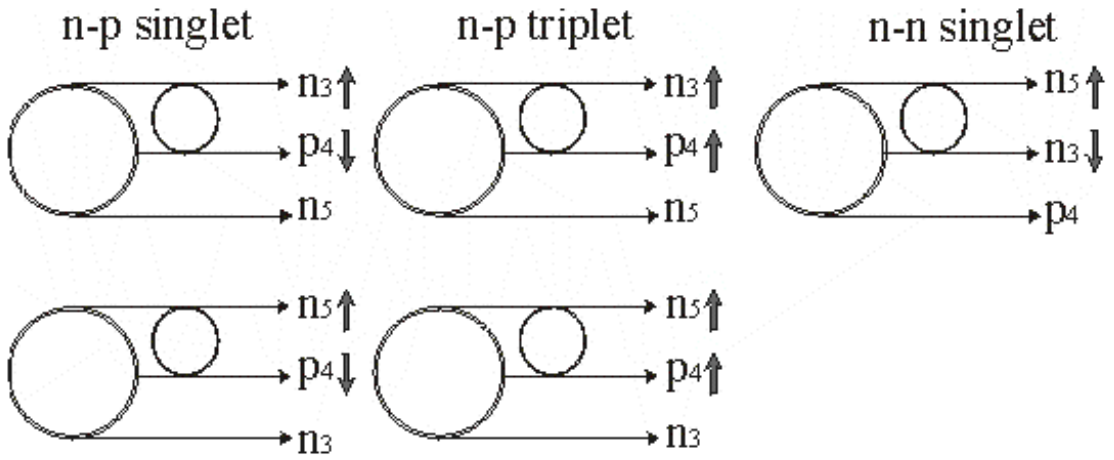
n-p singlet
n-p triplet
n-n singlet
n3
p4
n5
n5
p4
n3
n5
p4
n3
n3
p4
n5
n5
p4
n3

FIGURE 2

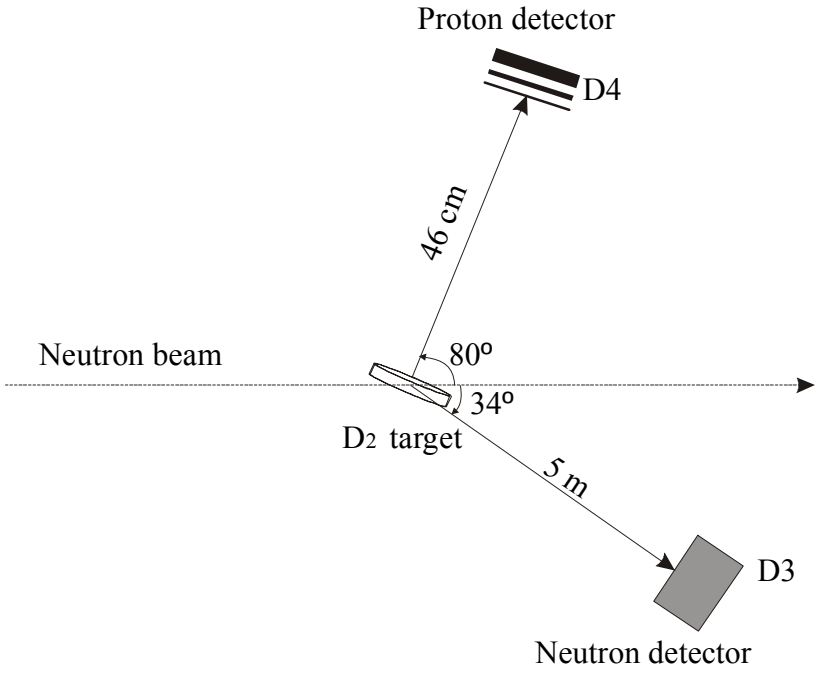
Proton detector
D4
46 cm
Neutron beam
80º
34º
D2 target
5 m
D3
Neutron detector

FIGURE 3

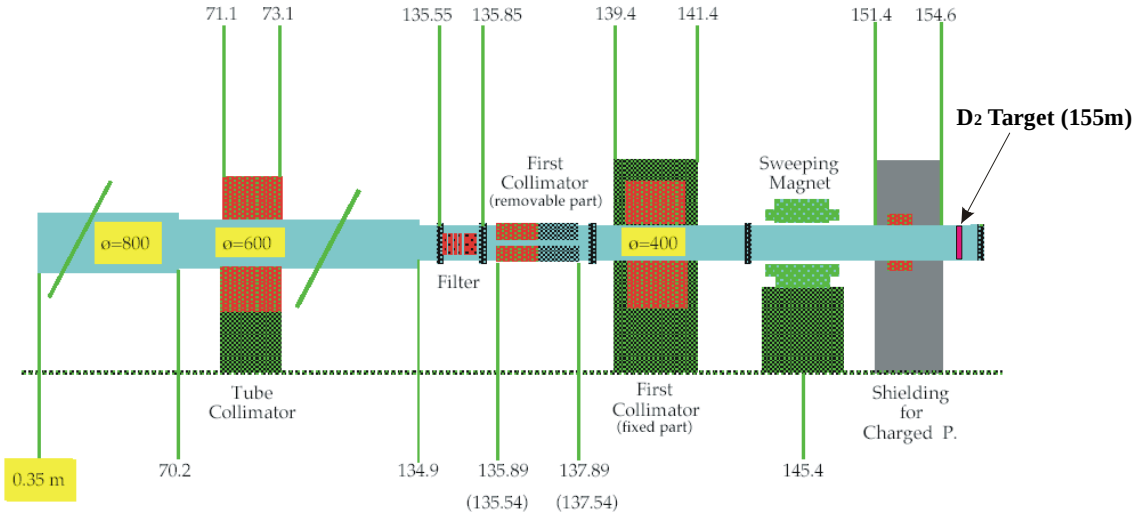
71.1
73.1
135.55
135.85
139.4
141.4
151.4
154.6
D2 Target (155m)
First
Collimator
(removable part)
Sweeping
Magnet
ø=800
ø=600
ø=400
Filter
Tube
Collimator
First
Collimator
(fixed part)
Shielding
for
Charged P.
0.35 m
70.2
134.9
135.89
(135.54)
137.89
(137.54)
145.4

FIGURE 4

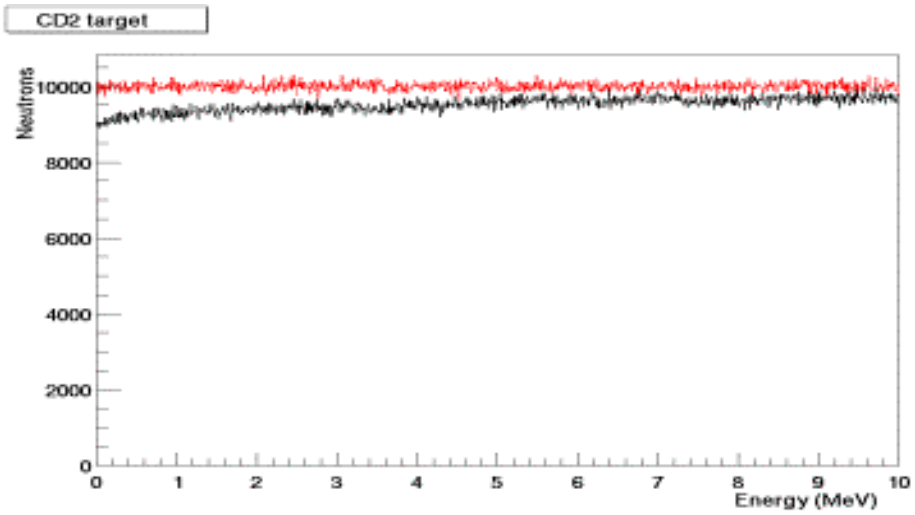
CD2 target
Neutrons
10000
8000
6000
4000
2000
0
0
1
2
3
4
5
6
7
8
9
10
Energy (MeV)

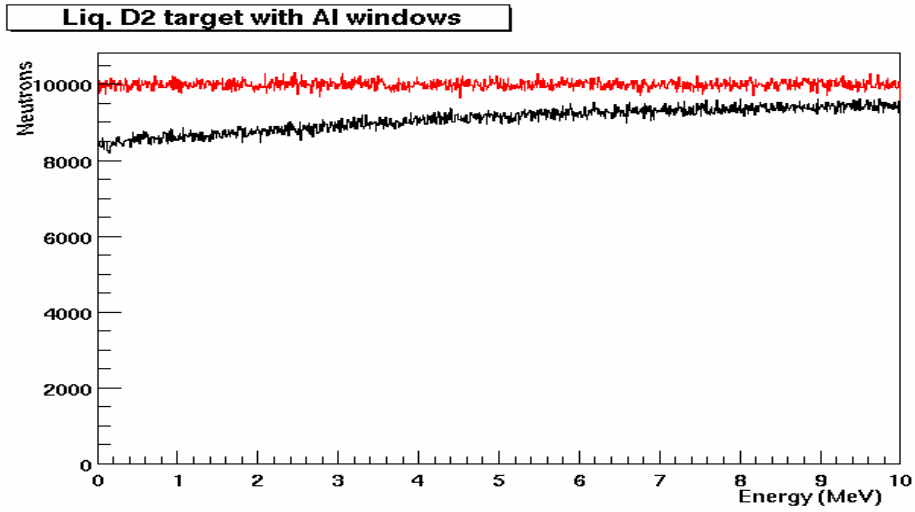
Liq. D2 target with Al windows
Neutrons
10000
8000
6000
4000
2000
0
0
1
2
3
4
5
6
7
8
9
10
Energy (MeV)

FIGURE 5

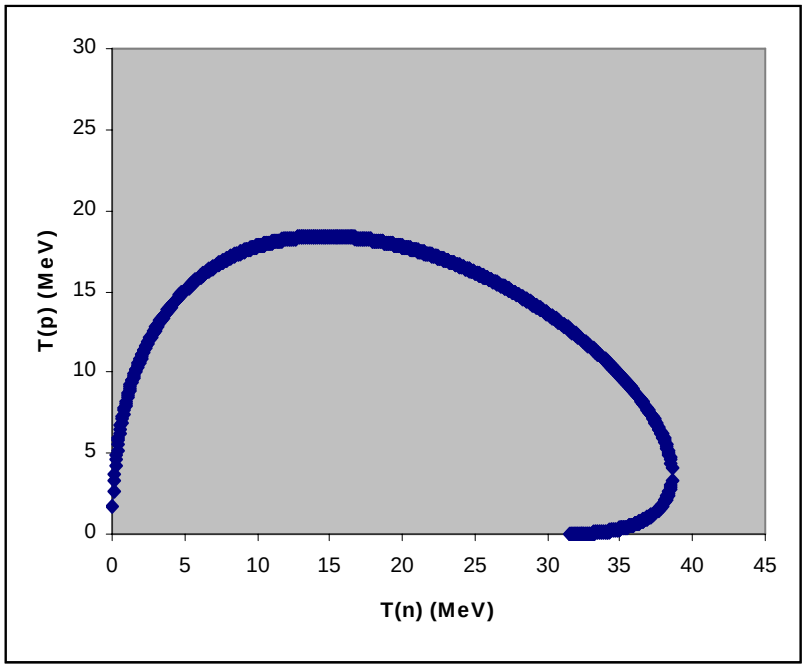

FIGURE 6

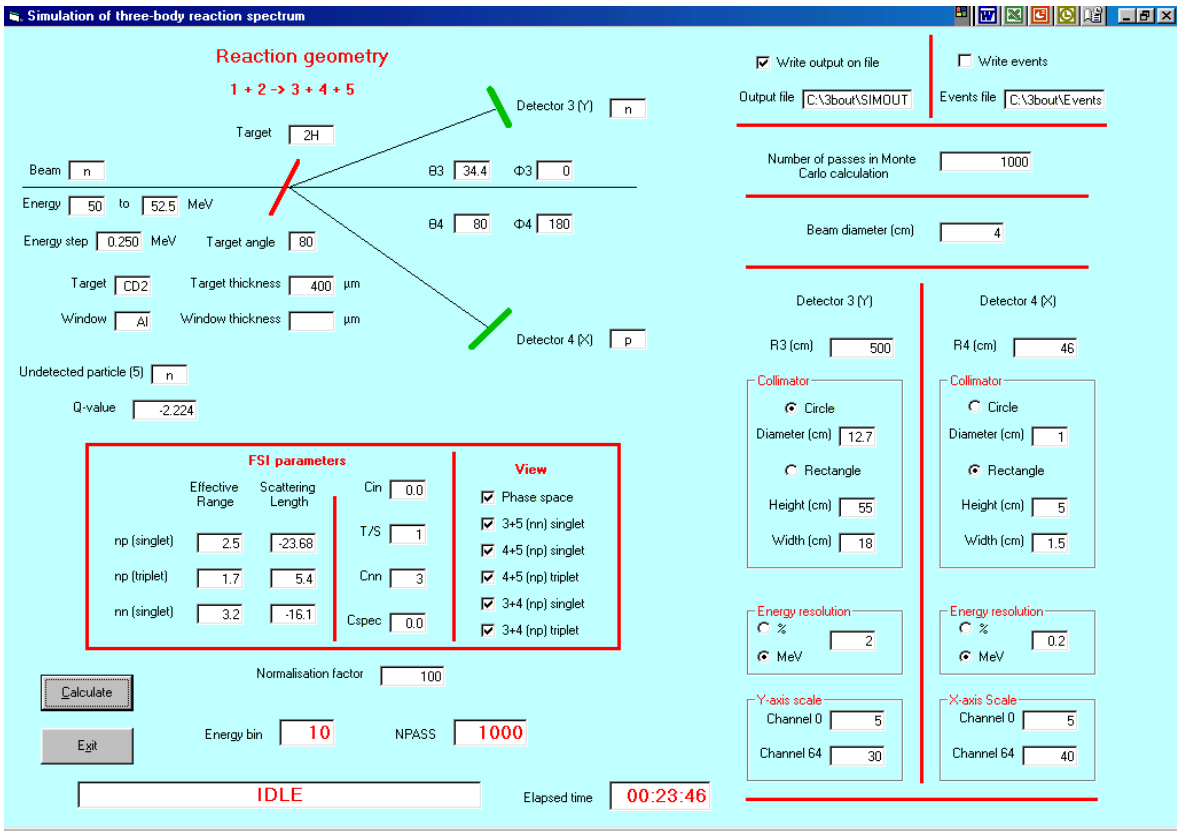
Simulation of three-body reaction spectrum
Reaction geometry
1 + 2 -> 3 + 4 + 5
Target 2H
Beam n
Energy 50 to 52.5 MeV
Energy step 0.250 MeV
Target angle 80
Target CD2
Target thickness 400 µm
Window Al
Window thickness µm
Undetected particle (5) n
Q-value -2.224
Detector 3 (Y) n
θ3 34.4 Φ3 0
θ4 80 Φ4 180
Detector 4 (X) p
FSI parameters
Effective Range
Scattering Length
np (singlet) 2.5 -23.68
np (triplet) 1.7 5.4
nn (singlet) 3.2 -16.1
Cin 0.0
T/S 1
Cnn 3
Cspec 0.0
View
Phase space
3+5 (nn) singlet
4+5 (np) singlet
4+5 (np) triplet
3+4 (np) singlet
3+4 (np) triplet
Normalisation factor 100
Calculate
Exit
Energy bin 10
NPASS 1000
IDLE
Elapsed time 00:23:46
Write output on file
Output file C:\3bout\SIMOUT
Write events
Events file C:\3bout\Events
Number of passes in Monte Carlo calculation 1000
Beam diameter (cm) 4
Detector 3 (Y)
R3 (cm) 500
Collimator
Circle
Diameter (cm) 12.7
Rectangle
Height (cm) 55
Width (cm) 18
Energy resolution
% 2
MeV
Y-axis scale
Channel 0 5
Channel 64 30
Detector 4 (X)
R4 (cm) 46
Collimator
Circle
Diameter (cm) 1
Rectangle
Height (cm) 5
Width (cm) 1.5
Energy resolution
% 0.2
MeV
X-axis Scale
Channel 0 5
Channel 64 40

FIGURE 7

```
n + 2H -> n + p + n

Energy range = 60 to 62.5 MeV

Theta1 =34.4
Theta2 =80

Beam diameter = 4 cm
Target angle = 80
Target; thickness = 400 µm

Detector 3(Y):
R = 500 cm
Collimator circle, diameter = 12.7 cm
Resolution = 2 MeV
Y axis energy scale: Channel 0 = 5 Channel 64 = 30 MeV

Detector 4(X):
R = 46 cm
Collimator rectangle, Height = 5, Width = 1.5 cm
Resolution = 0.2 MeV
X axis energy scale: Channel 0 = 5 Channel 64 = 40 MeV

Final state interaction parameters:
nn Singlet: Scattering Length = -16.1, Effective range = 3.2 fm
np Singlet: Scattering Length = -23.68, Effective range = 2.5 fm
np Triplet: Scattering Length = 5.4, Effective range = 1.7 fm
Cin = 0.0
T/S = 1
Cnn = 3
Cspec = 0.0

Passes in Monte Carlo calculation = 10000
```

FIGURE 8

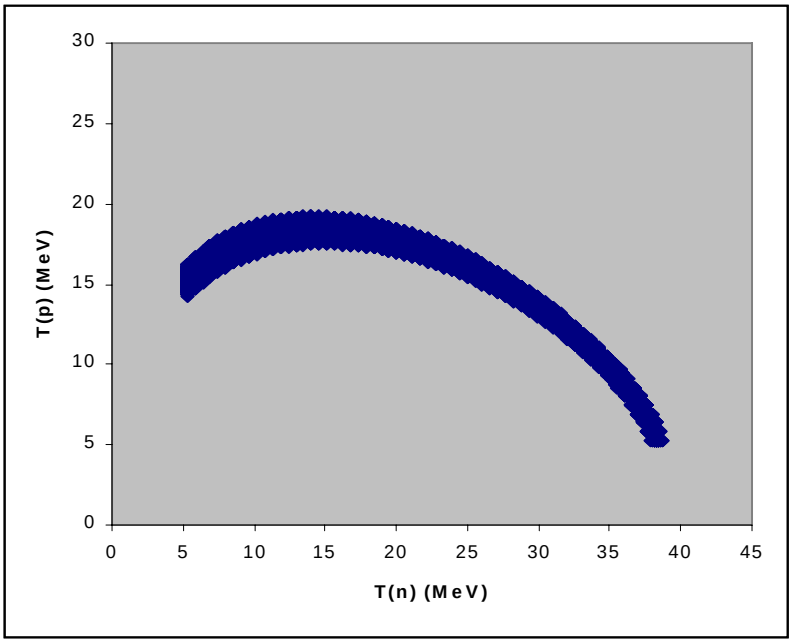
30
25
20
15
10
5
0
T(p) (MeV)
0
5
10
15
20
25
30
35
40
45
T(n) (MeV)

(a)

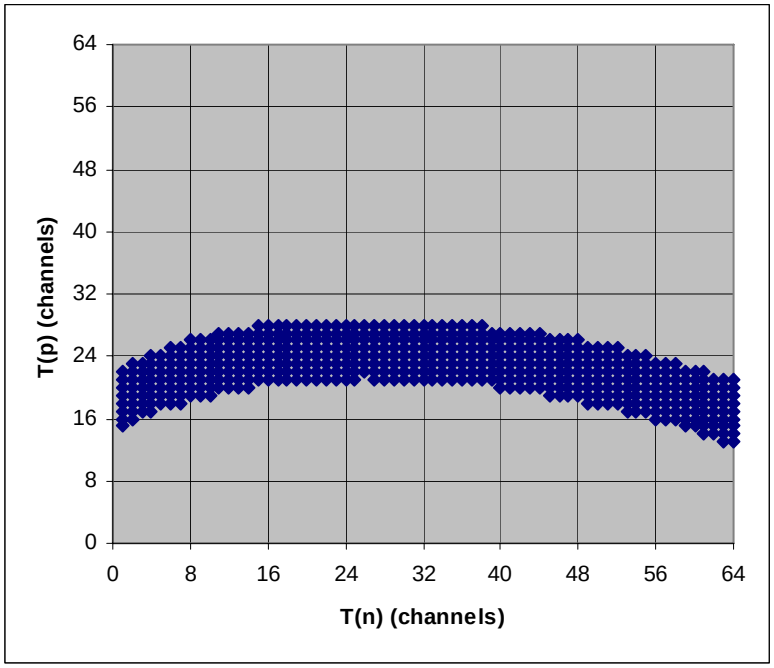
64
56
48
40
32
24
16
8
0
T(p) (channels)
0
8
16
24
32
40
48
56
64
T(n) (channels)

(b)

FIGURE 9

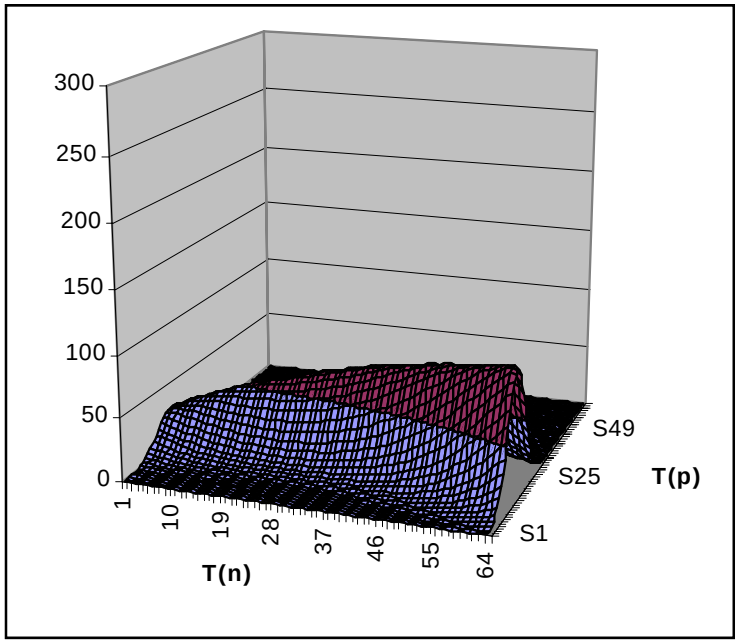
300
250
200
150
100
50
0
1
10
19
28
37
46
55
64
T(n)
S1
S25
S49
T(p)

(a)

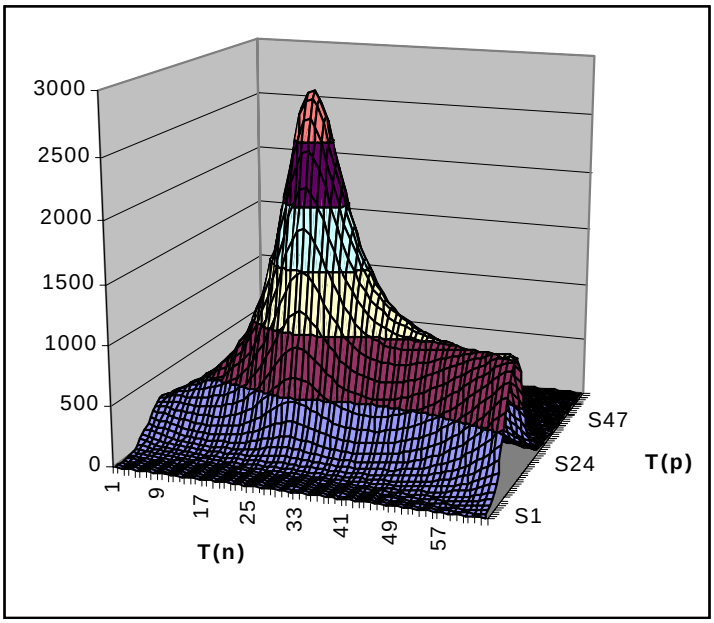
3000
2500
2000
1500
1000
500
0
1
9
17
25
33
41
49
57
T(n)
S1
S24
S47
T(p)

(b)

FIGURE 10

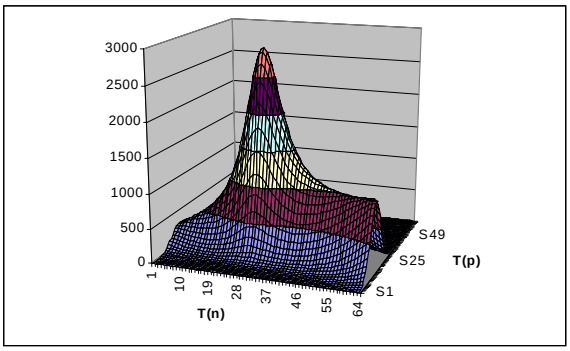

a_{nn} = - 16.1 fm

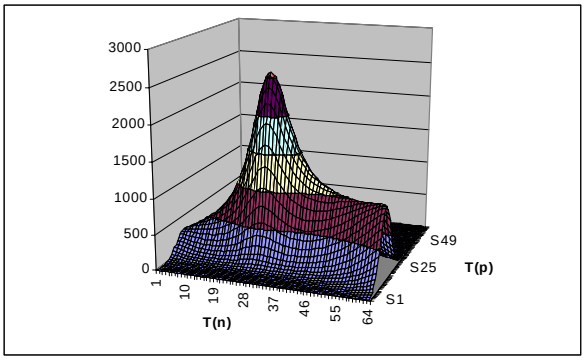

a_{nn} = - 15.1 fm

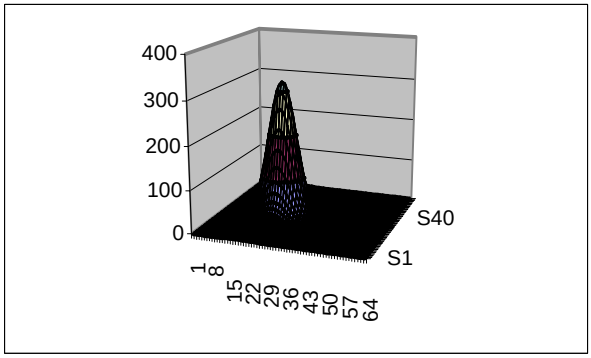

Difference

FIGURE 11

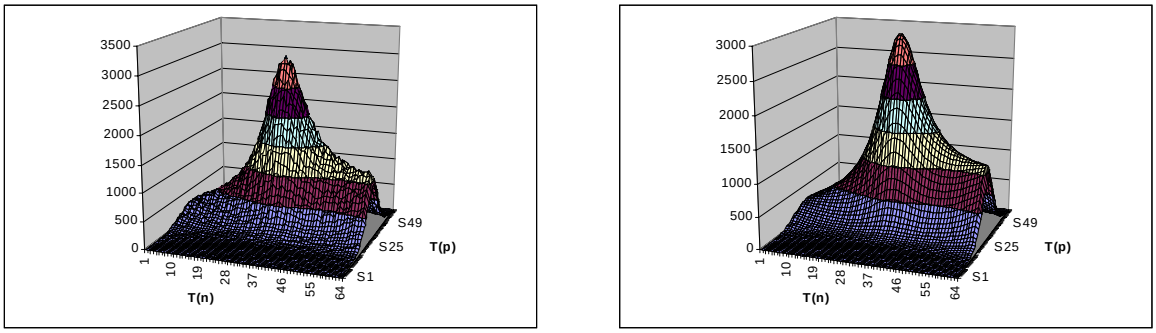
3500
3000
2500
2000
1500
1000
500
0
1
10
19
28
37
46
55
64
T(n)
S49
S25
S1
T(p)
3000
2500
2000
1500
1000
500
0
1
10
19
28
37
46
55
64
T(n)
S49
S25
S1
T(p)

FIGURE 12